AMERICAN SOCIETY FOR MICROBIOLOGY | Antimicrobial Agents and Chemotherapy®

ANTIVIRAL AGENTS

# Prophylactic Antiheparanase Activity by PG545 Is Antiviral *In Vitro* and Protects against Ross River Virus Disease in Mice

**Aroon Supramaniam,[a]* Xiang Liu,[a] Vito Ferro,[b,c] Lara J. Herrero[a]***

[a]Institute for Glycomics, Griffith University, Gold Coast Campus, Southport, QLD, Australia
[b]School of Chemistry and Molecular Biosciences, the University of Queensland, Brisbane, QLD, Australia
[c]Australian Infectious Diseases Research Centre, the University of Queensland, Brisbane, QLD, Australia

**ABSTRACT** Recently we reported on the efficacy of pentosan polysulfate (PPS), a heparan sulfate mimetic, to reduce the recruitment of inflammatory infiltrates and protect the cartilage matrix from degradation in Ross River virus (RRV)-infected PPS-treated mice. Here, we describe both prophylactic and therapeutic treatment with PG545, a low-molecular-weight heparan sulfate mimetic, for arthritogenic alphaviral infection. We first assessed antiviral activity *in vitro* through a 50% plaque reduction assay. Increasing concentrations of PG545 inhibited plaque formation prior to viral adsorption in viral strains RRV T48, Barmah Forest virus 2193, East/Central/South African chikungunya virus (CHIKV), and Asian CHIKV, suggesting a strong antiviral mode of action. The viral particle-compound dissociation constant was then evaluated through isothermal titration calorimetry. Furthermore, prophylactic RRV-infected PG545-treated mice had reduced viral titers in target organs corresponding to lower clinical scores of limb weakness and immune infiltrate recruitment. At peak disease, PG545-treated RRV-infected mice had lower concentrations of the matrix-degrading enzyme heparanase in conjunction with a protective effect on tissue morphology, as seen in the histopathology of skeletal muscle. Enzyme-linked immunosorbent assay quantification of cartilage oligomeric matrix protein and cross-linked C-telopeptides of type II collagen as well as knee histopathology showed increased matrix protein degradation and cartilage erosion in RRV-infected phosphate-buffered saline-treated mice compared to their PG545-treated RRV-infected counterparts. Taken together, these findings suggest that PG545 has a direct antiviral effect on arthritogenic alphaviral infection and curtails RRV-induced inflammatory disease when administered as a prophylaxis.

**KEYWORDS** GAGs mimetics, alphaviruses, anti-inflammatory, athritogenic, heparan sulfate mimetics

Ross River virus (RRV) is a clinically relevant mosquito-borne arthritogenic arbovirus from the *Togaviridae* family, *Alphavirus* genus, together with chikungunya virus (CHIKV), Sindbis virus (SINV), and Barmah Forest virus (BFV) (1). The typical RRV clinical presentation is characterized by the sudden onset of fever, maculopapular rash, and musculoskeletal pain with lethargy in patients with RRV disease (RRVD). Certain patients (approximately 40 to 60% of sufferers) progress to a persistent debilitative form of a chronic inflammatory arthralgia with agonizing pain (2, 3).

RRVD remains a notifiable disease, in addition to being the largest contributor to the annual disease burden ($n$ = 5,000) of arboviral infections in Australia (4, 5). Recently, rapid globalization has facilitated the spread of CHIKV from the Eastern to the Western Hemisphere, with outbreaks occurring from 2005 to 2017 (6). Despite the relevance and importance of these infectious arthritic diseases, there still lies an unmet therapeutic gap of a targeted treatment given the unsuitability of nonsteroidal anti-inflammatory drugs or steroid treatments for certain patient cohorts.

**Received** 29 September 2017 **Returned for modification** 25 October 2017 **Accepted** 15 January 2018

**Accepted manuscript posted online** 5 February 2018

**Citation** Supramaniam A, Liu X, Ferro V, Herrero LJ. 2018. Prophylactic antiheparanase activity by PG545 is antiviral *in vitro* and protects against Ross River virus disease in mice. Antimicrob Agents Chemother 62:e01959-17. https://doi.org/10.1128/AAC.01959-17.



Address correspondence to Lara J. Herrero, l.herrero@griffith.edu.au.

* Present address: Aroon Supramaniam and Lara J. Herrero, Institute for Glycomics, Griffith University, Queensland, Australia.

Previous studies on CHKV disease (CHIKVD) and RRVD in mice and human subjects have determined clinical disease to be exacerbated by inflammatory immunocytes, such as monocytes, macrophages, or neutrophils. For example, an initial study on the synovial exudates of RRVD patients reported the presence of 35% mononuclear infiltrates in the joint space of these patients (7). Moreover, other studies on CHIKV reported that treating CHIKV-infected mice with bindarit, a monocyte chemotactic protein 1 (MCP-1; CCL2) inhibitor, reduced the bone loss and muscle degradation seen in CHIKV-infected mice (8, 9). Recently a study described that in the absence of CCR2 receptors in the mouse model, the usual monocyte-macrophage profile shifts to a neutrophil-dominated pathogenic response (10).

We recently found the levels of heparanase (HPSE), an endoglycosidase found at basal homeostatic levels in immune cells such macrophages and neutrophils, to be upregulated in RRV-infected primary human chondrocytes and primary human skeletal muscle cells (11). HPSE acts primarily to cleave heparan sulfate (HS) molecules and has been found to contribute to inflammation-driven pathology in a range of human diseases (for a recent review, see reference 12), such as inflammatory bowel disease (IBD), cancer, and even rheumatoid arthritis (RA) (13–15). A study on RA found that both active heparanase and the transcript levels of the enzyme were elevated greater than 100-fold in the synovial fluid of patients (14). Furthermore, like the pathology of other inflammatory musculoskeletal disorders, such as osteoarthritis (OA) and RA, where progressive depletion of proteoglycans occurs in the affected articular cartilage, cartilage degradation has also been reported in both RRV- and CHIKV-infected mice (10, 16, 17). Notably, we previously found that at peak RRVD, ankle joints of mice undergo thinning of articular cartilage with the inclusion of a thickened pannus (16). Our laboratory recently established that repurposing pentosan polysulfate (PPS), already used as a disease-modifying drug to treat canines with OA, should also be investigated to treat human arthritogenic alphaviral diseases (18). We found that PPS treatment of both CHIKV- and RRV-infected mice resulted in disease amelioration and cartilage protection. As such, PPS has progressed to a phase 2 clinical trial that is currently ongoing, targeted to long-term RRV patients (16).

The therapeutic discovery of PPS provided the basis for the current study. We sought to expand the repertoire of HS mimetics and determine if HS mimetics could be a class of disease-modifying therapeutics for arthritogenic, alphaviral diseases such as RRVD. We strategically chose PG545 (19, 20), a drug candidate recently in phase 1 clinical trials in cancer patients (ClinicalTrials registration no. NCT02042781), with an anti-heparanase and anti-inflammatory therapeutic profile. Additionally, recent publications on PG545 report the compound demonstrates antiviral effects on HS binding viruses (21–24). Arthritogenic alphaviruses have been reported to initiate entry through HS binding on host cells (25, 26). In this study, we show that PG545 treatment worked effectively as a prophylaxis to alphaviral infection in mice and cells. RRV disease abatement occurred through both the reduction of viral particles as well as a dampened immune response with an overall reduction in tissue damage. We also noticed a reduced loss of articular cartilage and epiphyseal growth plate that otherwise occurs with RRV-mediated arthritis. Furthermore, we confirm our previous data, of the upregulation of heparanase in RRV-infected human primary cells, by showing upregulation of HPSE in RRVD mice. Overall, we conclude that PG545 is an effective anti-heparanase prophylactic treatment for arthritogenic alphaviral infections.

## RESULTS

**PG545 demonstrates efficient dose-dependent plaque inhibition on alphavirus-infected Vero cells.** To test antiviral effects and determine the required compound dose to achieve a 50% plaque inhibition, various concentrations of PG545 (42.3 $\mu$M [100 $\mu$g/ml], 8.46 $\mu$M [20 $\mu$g/ml], 1.69 $\mu$M [4 $\mu$g/ml], 0.34 $\mu$M [0.8 $\mu$g/ml], and 0.068 $\mu$M [0.16 $\mu$g/ml]) were coincubated with viral isolates before viral adsorption. As a control, we also investigated the plaque inhibition ability of PG545 when used after viral adsorption to host cell. The results (Fig. 1Ai to Di and Table 1) demonstrate that PG545

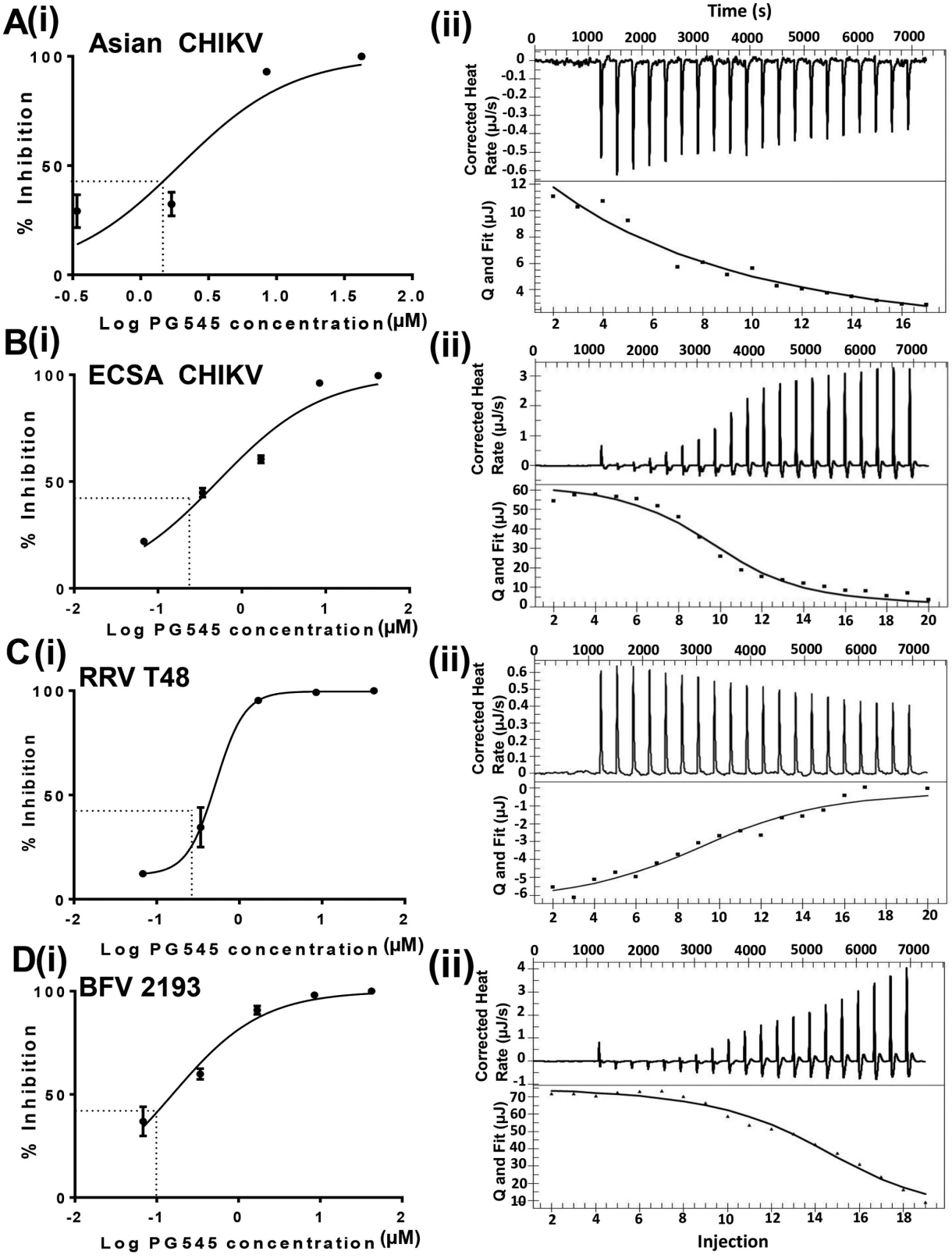


**FIG 1** PG545 binds to arthritogenic alphaviruses and inhibits productive infection of Vero cells in a dose-dependent manner at previral adsorption. (Ai to Di) Fivefold dilutions of PG545 were coincubated with viral strains (RRV T48, chikungunya East/Central/South African virus [CHIKV ESCA], Asian CHIKV, and BFV2193) and then assayed for overall plaque formation. $IC_{50}$ dose was determined by normalizing plaques to mock-infected controls. (Aii to Dii) The corresponding thermodynamic graphs of PG545 binding to virus, where upper panels show raw heat of ligand binding while lower panels show binding isotherms fitted to the raw data using a single-state binding model. Q, heat.

**TABLE 1** Binding profile between athritogenic alphaviruses and PG545

| Virus strain (laboratory adapted) | $IC_{50}$ ($\mu$M)[a] | | $K_D$ ($\mu$M) | $n^b$ |
|---|---|---|---|---|
| | Preadsorption | Postadsorption | | |
| Asian CHIKV | 1.94 (±2.69) | 8.50 (±0.18) | 4.01 (±0.42) | 0.75 (±0.45) |
| ECSA CHIKV | 0.51 (±0.50) | 26.8 (±11.05) | 0.35 (±0.22) | 1.47 (±0.34) |
| RRV T48 | 0.52 (±0.36) | 15.35 (±8.50) | 0.34 (±0.19) | 2.26 (±0.91) |
| BFV 2193 | 0.16 (±0.01) | 8.12 (±3.76) | 0.25 (±0.12) | 1.10 (±0.05) |

[a]$IC_{50}$ determinations were done on the various virus strains at preadsorption and postadsorption stages using virus plaque inhibition assays. The binding constant ($K_D$) and the number of binding sites in viral proteins were calculated using isothermal calorimetry titration, where binding parameters were calculated thermodynamically. All values in the table are represented as means ± SEM from 2 or 3 independent experiments.

[b]*n*, number of active binding sites in viral protein.

reduced the plaque-forming ability of the various athritogenic alphaviral strains effectively prior to viral adsorption, with $IC_{50}$ (half maximum inhibitory compound concentration) values ranging from 1.94 $\mu$M (4.57 $\mu$g/ml) to 0.16 $\mu$M (0.37 $\mu$g/ml). However, when treatment was initiated after viral adsorption, plaque inhibition was poor (Table 1; see also Fig. S1 in the supplemental material).

We next characterized the binding interactions between PG545 and whole virus by isothermal titration calorimetry (ITC) (Fig. 1Aii to Dii and Table 1), evaluating the stoichiometry (binding sites) and binding constants ($K_D$; i.e., the thermodynamic binding constant representing the dissociation/association ratio of compound to virus). Figure 1Aii to Dii shows thermodynamic parameters of PG545 binding to virus variants. Overall the $K_D$ values ranged from 4.01 (±0.42) $\mu$M to 0.25 (±0.12) $\mu$M, demonstrating efficient binding affinity of PG545 to the viral proteins. This efficient binding correlates with the $IC_{50}$ data, which show the ability of PG545 to inhibit virus to nanomolar ranges.

**Prophylactic PG545 treatment reduces the severity of clinical signs and RRV-induced inflammation.** To assess PG545 as a treatment strategy for RRV disease, mice were preloaded with PG545 subcutaneously (s.c.) at 20 mg/kg of body weight and then infected with RRV or mock infected with phosphate-buffered saline (PBS) alone. Mice were then treated with a second dose of PG545 at 10 mg/kg within a 10-day time frame (Fig. 2Ai). This prophylactic treatment regimen resulted in a significant reduction of disease scores at 8 days postinfection (dpi) (*P* value of $<0.05$), 9 dpi (*P* value of $<0.01$), and 10 dpi (*P* value of $<0.05$) in the RRV-infected PG545-treated group, in addition to a comparable reduction in RRVD-induced weight loss at 8 (*P* value of $<0.05$), 9 (*P* value of $<0.01$), and 10 (*P* value of $<0.001$) dpi (Fig. 2Aii and iii). To further evaluate the reduction in clinical disease, the inflammatory response and histopathology of RRV-infected PBS- and PG545-treated mice were compared. Muscles from RRV-infected PBS- or PG545-treated mice were harvested at peak disease (10 dpi) for both histology (Fig. 2Bi and ii) and flow cytometry (Fig. 2Ci and ii). Predictably, the control muscle tissues were only sparsely populated with immune cells, with well-preserved muscle fiber architecture for mock-infected PBS control (mean count of 555.50 ± 67.5), or mock-infected PG545-treated (mean count of 623.25 ± 42.96) samples (Fig. 2Bii). Supporting other studies, RRV-infected PBS-treated mice presented with characteristic impairment of the longitudinal muscular fibrils in addition to marked polymorph nuclear leukocytic accumulation (mean count of 2,359.25 ± 345.63) (Fig. 2Bii). Notable necrotic fibers scattered and separated by dense immunocytes were also observed in the RRV-infected PBS-treated group. In contrast, RRV-infected PG545-treated mice displayed muscle fiber morphology with cross striations and no necrosis. In addition, there were lower numbers of infiltrating immune cells than those for the RRV-infected PBS-treated group (mean count of 703.25 ± 34.53) (Fig. 2Bii). To characterize the effect of PG545 treatment on both lymphocytic and myeloid cell populations, the leukocyte subset response within the muscles was analyzed by flow cytometry. The RRV-infected PBS-treated or RRV-infected PG545-treated myocytes were stained for Gr-1$^+$ CD11b$^+$ and CD3$^+$ cell surface antigen markers found on granulocytes (neutrophils), monocytes, and T cells. At

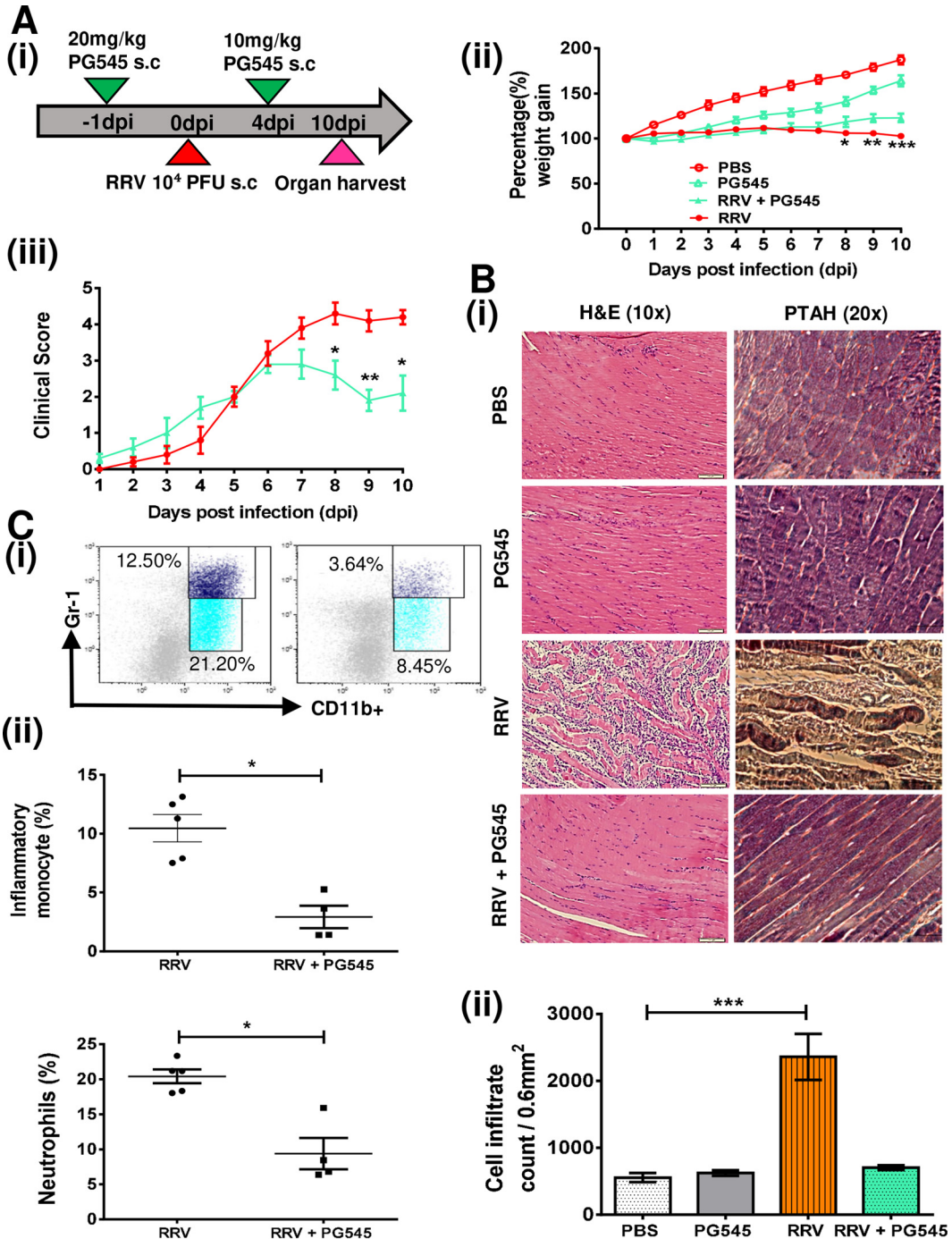


**FIG 2** Prophylactic PG545 treatment ameliorates RRVD in mice at peak disease. (Ai) C57BL/6 mice were infected (s.c.) with $10^4$ PFU/50 $\mu$l RRV or PBS alone on day 0 and received s.c. injections of PG545 or PBS diluents from on day −1 and day 4 after infection. (Aii and iii) Mice were weighed and scored for disease progression as described in Materials and Methods. (Bi) Muscles were fixed in 4% PFA and H&E or PTAH stained. (Bii) Total cell infiltrates were counted using Image J and then graphed. (Ci and ii) Enzymatically digested muscle homogenates were stained for neutrophils ($Gr1^{+/high}$ $CD11b^{+/high}$) and inflammatory monocytes ($Gr1^{+/mid}$ $CD11b^{+/high}$). Each data point represents the means ± SEM from 4 to 6 mice and is representative of 2 or 3 independent experiments. PBS, mock-infected PBS control; PG545, mock infected and PG545 treated; RRV, RRV infected and PBS treated; RRV + PG545, RRV infected and PG545 treated.

10 dpi, PG545 treatment significantly ($P$ value of $<0.05$) (Fig. 2Cii) reduced the percentages of Gr-$1^{+/high}$ $CD11b^{+/high}$-expressing inflammatory monocytes and Gr-$1^{+/mid}$ $CD11b^{+/high}$-expressing neutrophils in RRV-infected PG545-treated mice (inflammatory monocytes, mean reduction of 2.92% ± 0.95%; neutrophils, mean reduction of 9.39% ±

2.23%) compared to the RRV-infected PBS-treated mice group (inflammatory monocytes, mean of 10.47% ± 1.17%; neutrophils, mean of 20.42% ± 0.99%). Interestingly, PG545 treatment did not alter the $CD3^+$ lymphocytic T-cell response between the RRV-infected PG545-treated (mean of 32.94% ± 3.55%) and RRV-infected PBS-treated groups (mean of 31.78% ± 2.11%) (data not shown).

**Prophylactic PG545 treatment reduces RRV load in target tissues.** To evaluate the antiviral potency of prophylactic PG545 treatment *in vivo*, viral titers and viral load were measured from joints, muscles, and serum of RRV-infected PG545-treated and RRV-infected PBS-treated mice groups at 1, 3, 5, 7, and 10 dpi. Serum and ankle titers at 3 dpi showed reduced titers in RRV-infected PG545-treated mice that were statistically significant (Fig. 3Bi [*P* value of $<0.05$] and ii [*P* value of $<0.0001$]) compared to the RRV-infected PBS-treated mice. Whereas other time points showed an overall reduction in viral titer, no statistical significance was noted; however, a generally dampened kinetic pattern was observed in RRV-infected PG545-treated mice from 7 dpi to 10 dpi in ankles and 5 dpi to 7 dpi in muscles.

To assess the reduction of viral RNA, quantitative PCR (qPCR) was performed. The results demonstrated reduction in residual virus load in both muscles and joints of RRV-infected PG545-treated mice compared to RRV-infected PBS-treated mice at 7 dpi and 10 dpi, coinciding with disease onset.

**Prophylactic PG545 treatment downregulates the expression levels of proinflammatory soluble host mediators in target organs of RRV-infected mice.** Soluble inflammatory host factors are known to modulate inflammatory responses and aid in the activation or recruitment of various inflammatory leukocyte subsets in alphaviral pathology. Since the infiltration of immunocytes was dampened in the RRV-infected PG545-treated group compared to that of the RRV-infected PBS-treated group, as seen in flow cytometry and H&E staining, we decided to further assess the expression levels of host factors which play an important role in both viral infection and inflammation. Cytokine gene expression studies revealed that mRNA levels of proinflammatory tumor necrosis factor alpha (TNF-$\alpha$), interleukin-6 (IL-6), vascular endothelial growth factor A (VEGF-A), gamma interferon (IFN-$\gamma$), and MCP-1 were all markedly lower in RRV-infected PG545-treated groups than in RRV-infected PBS-treated groups. Interestingly, while the mock-infected PG545-treated group showed trends similar to those of the mock-infected PBS group, PG545 treatment did show a statistically significant elevation of VEGF-A (*P* value of $<0.0001$) (Fig. 4) and TNF-$\alpha$ (*P* value of $<0.0001$) (see Fig. 9) in the joints compared to levels for the PBS treatment group.

Expression levels of MCP-1 in both muscle and joint was significantly (*P* value of $<0.0001$) (Fig. 4) lower in the RRV-infected PG545-treated group than in the RRV-infected PBS-treated group. Reduction in gene expression was also detected for IL-6 (muscle, *P* value of $<0.01$; joint, *P* value of $<0.0001$), IFN-$\gamma$ (muscle, *P* value of $<0.05$; joint, *P* value of $<0.001$), and TNF-$\alpha$ (muscle, *P* value of $<0.0001$) in RRV-infected PG545-treated groups. Expression levels of TNF-$\alpha$ in joints showed a modest elevation in the RRV-infected PBS-treated group (mean fold increase of 3.94 ± 0.29), with a consistent trend of lower expression noted in the RRV-infected PG545-treated joint (mean fold decrease of 3.75 ± 0.25). Interestingly, the overall expression levels of VEGF-A, in both joint (mean fold increase of 0.76 ± 0.06) and muscles (mean fold increase of 0.50 ± 0.12), were higher in RRV-infected PG545-infected mice than in RRV-infected PBS-treated groups (joint, mean fold decrease of 0.67 ± 0.03; muscle, mean fold decrease of 0.19 ± 0.02), with statistical significance of a *P* value of $<0.5$ (Fig. 4) noted for the muscles. Overall, these findings were consistent with other previously published data, which have shown that lowering viremia by antiviral drug treatments could also reduce the acute inflammatory response, as represented by reduction in proinflammatory cytokine levels (27, 28).

**Prophylactic PG545 treatment reduces HPSE levels in mice.** HPSE, the extracellular matrix (ECM)-degrading enzyme, had higher fold expression in the RRV-infected PBS-treated joint at a mean of 2.00 ± 0.09 (*P* value of $<0.0001$) than in the RRV-infected

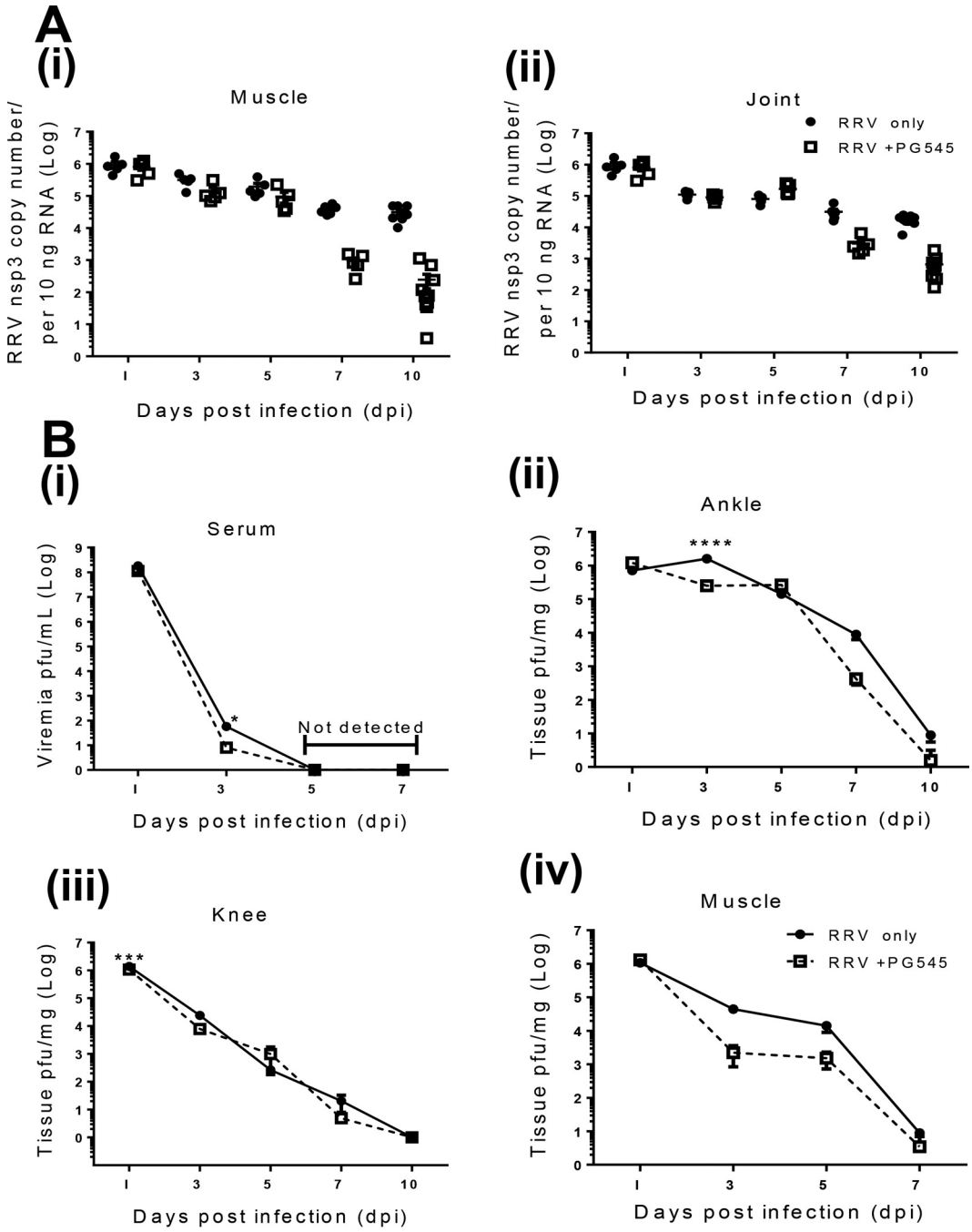


**FIG 3** Prophylactic PG545 treatment deters RRV replication and influences the reduction of viral genomic material at target tissues. Twenty-one-day-old C57BL/6 RRV-infected mock-treated or RRV-infected PG545-treated mice were infected subcutaneously (s.c.) with $10^4$ PFU RRV in the right thorax. At 1, 3, 5, 7, and 10 dpi, serum, muscle, ankles, and knees were harvested. Muscle and joint tissues were homogenized for plaque assay and/or RNA extracted for viral genomic material analysis. (Ai and ii) To determine viral load within the musculoskeletal tissues, plasmid copy numbers were extrapolated from RRV T48 standards ($n = 7$) with the qPCR detection limit set at 38 copies of viral RNA transcript per 10 ng template. (Bi to iv) The amounts of infectious virus in tissues and serum were titrated in Vero cells and expressed as PFU/mg or PFU/ml, with the lower plaque detection limit set at 50 PFU/ml. Data points are displayed as means ± SEM for 4 to 10 mice per treatment group. PFU, PFU per milliliter. RRV, RRV infected and PBS treated; RRV + PG545, RRV infected and PG545 treated.

PG545-treated group (mean fold of 1.13 ± 0.08) (Fig. 5ii). As noted in our previous human primary cell study (11), HPSE was also upregulated in RRV-infected PBS-treated muscles at a mean fold increase of 3.66 ± 0.23, while PG545 treatment of RRV-infected mice showed significantly ($P$ value of $<0.05$) reduced HPSE expression at a mean fold

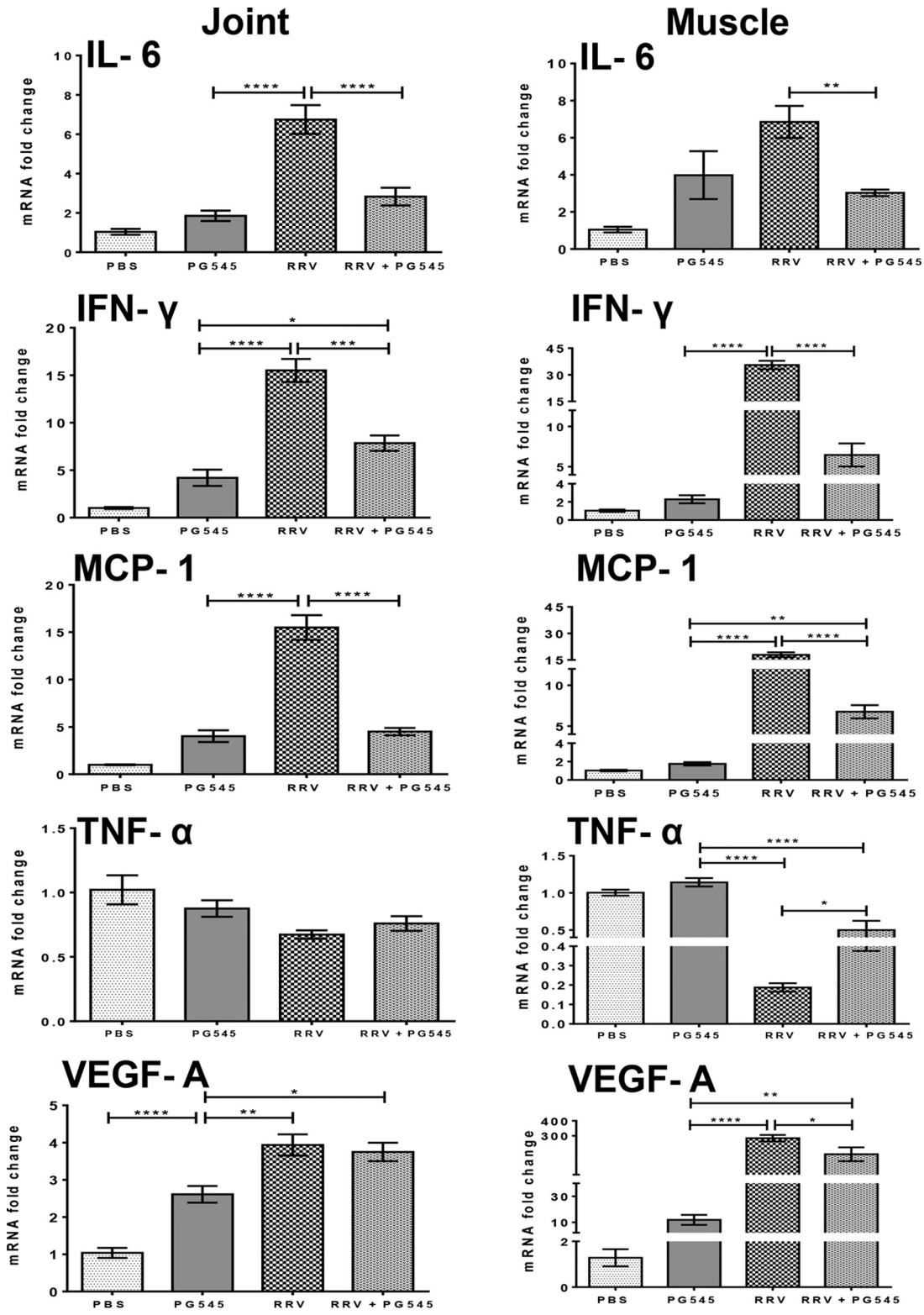


**FIG 4** Prophylactic PG545 treatment reduces upregulation of soluble host factors in RRVD mice. Muscles and joints were homogenized and RNA extracted to analyze soluble host factor expression via qPCR. The *y* axis is the final calibrated transcript expression graphed as fold shift, and the *x* axis designates the treatment groups. PBS, mock-infected PBS control; PG545, mock infected and PG545 treated; RRV, RRV infected and PBS treated; RRV + PG545, RRV infected and PG545 treated. Values are expressed as mean ± SEM mRNA fold changes in expression for 4 or 5 mice in each group.

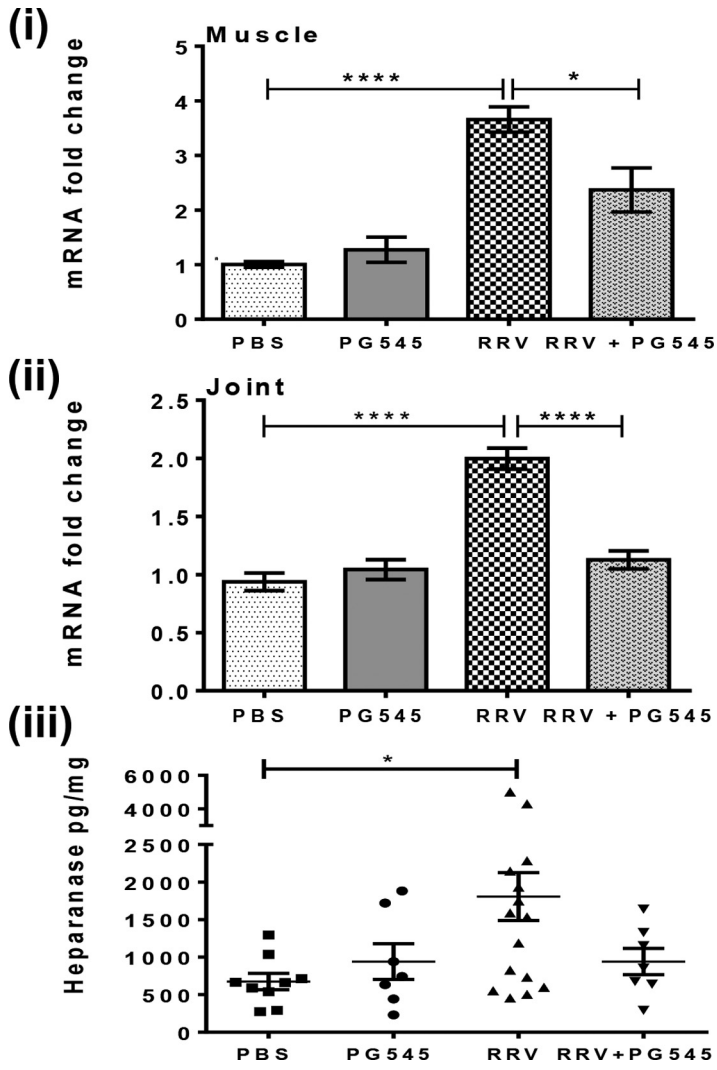


**FIG 5** Prophylactic PG545 treatment reduces HPSE. (i to iii) Muscles and joints were homogenized for ELISA and/or RNA extracted for qPCR analysis as described previously. The *y* axis is the final calibrated transcript expression graphed as fold shift, and the *x* axis designates the treatment groups. (iii) PBS-homogenized muscle lysates were assayed for use in a commercial sandwich ELISA kit. OD readings were extrapolated against a set of 7 standards to determine protein concentrations in pg/mg. Values are expressed as means ± SEM from 4 to 17 mice per group. PBS, mock-infected PBS control; PG545, mock infected and PG545 treated; RRV, RRV infected and PBS treated; RRV + PG545, RRV infected and PG545 treated. HPSE, heparanase.

decrease of 2.37 ± 0.40 (Fig. 5i). Further, enzyme-linked immunosorbent assay (ELISA) quantification of HPSE protein levels in muscles (Fig. 5iii) confirmed the transcriptional profile seen in Fig. 5i, with a *P* value of $<0.01$ between the infected mock-treated and infected compound-treated group. This suggests a prominent role of HPSE in exacerbating RRVD, as recently reported for RA and other inflammatory-mediated pathogeneses.

**Prophylactic PG545 treatment protects cartilage from damage associated with RRVD.** Recently, RRVD was shown to induce both bone and joint pathology through the loss of articular cartilage and thinning of epiphyseal growth plates. This is in addition to the widespread bone loss of the vertebrae and long bones in RRV-infected mice. It was also reported that PPS, a relevant HS mimetic, is protective against the loss of proteoglycan matrix in both the articular surfaces and epiphyseal growth plates in the joints of RRV-infected mice. Thus, this study sought to further detail if these chondroprotective effects could be induced by other comparable HS mimetics. In

agreement with the PPS study, our findings also show both surface and subsurface articular irregularities in peak RRVD, which were reduced with PG545 treatment. While mock-infected PBS control and mock-infected PG545-treated samples stained evenly for Safranin O (SAFO) at their tibiofemoral articular surfaces, RRV-infected PBS-treated samples stained unevenly, with variations in the proteoglycan distribution within the articular topology. Moreover, RRV-infected PBS-treated groups demonstrated cartilage erosion (Fig. 6Ai, black arrows) at their anterior lateral tibial cartilage regions, exposing the underlying subchondral bones. Interestingly, there were also higher frequencies of diffusely spread hypertrophic chondrocytes found along the articular surfaces in these animals, while only infrequent hypertrophic chondrocytes were seen in control groups. Curiously, the anterior lateral meniscus in RRV-infected PBS-treated mice was also observed to be rich in proteoglycan content with high numbers of infiltrating fibrochondrocytes, which were observed to a lesser extent in the other groups. In contrast, RRV-infected PG545-treated mice did not experience a loss or weakening of their proteoglycan staining index. Quantification of the joint interface at lateral femur and lateral articular cartilage showed an overall reduction ($P$ value of $<0.05$) in cartilage thickness index in RRV-infected PBS-treated mice compared to that of RRV-infected PG545-treated mice in the tibial articular compartment (Fig. 6Aii and iii). Moreover, the systemic concentrations of cartilage oligomeric matrix protein (COMP) and cross-linked C-telopeptides of type II collagen (CTX-II) (Fig. 6B) in the serum were also significantly higher ($P$ value of $<0.01$) in the RRV-infected mock-treated group than in the RRV-infected PG545-treated group.

**Prophylactic PG545 treatment protects growth plate thinning associated with RRV disease.** As previously reported in our earlier studies (16), a similar reduction in the tibial epiphyseal growth plate width in the RRV-infected PBS-treated mice (Fig. 7Ai and ii) was also observed. Moreover, all three zonal regions of the growth plate in the RRV-infected PBS-treated mice were also highly reduced (Fig. 7Aii). As expected, this effect of cartilage atrophy was significantly less in RRV-infected PG545-treated mice (coronal plane, $P$ value of $<0.0001$; sagittal plane, $P$ value of $<0.01$). Figure 7Bi and ii shows that PG545 protects against the RRV-associated growth plate width reduction.

**Therapeutic administration of PG545 does not modify the clinical disease in RRV-infected mice but weakly reduces viral load in target organs.** Following success in prophylactic treatment with PG545 for RRVD in mice, the outcomes of PG545 treatment after RRV exposure at onset of disease and at peak viremia (described in previous studies as 2 dpi in RRV-infected mice [29, 45]) were examined. Mice were infected with RRV or mock infected with PBS alone and then treated s.c. with either PG545 or PBS at 20 mg/kg for the first dose at 3 dpi, and thereafter a second dose of 10 mg/kg was given at 7 dpi (Fig. 8Ai). This therapeutic treatment regimen resulted in no observable difference in clinical disease between the RRV-infected PG545-treated and RRV-infected PBS-treated groups (Fig. 8Aiii). Interestingly, despite the overall indifference to disease scores, a significant RRVD-induced weight loss ($P$ value of $<0.05$) was observed in RRV-infected PBS-treated mice compared to weights of RRV-infected PG545-treated mice at 10 dpi (Fig. 8Aii). Further, therapeutic PG545 treatment still reduced cellular infiltrate accumulation in muscles in RRV-infected PG545-treated mice (mean count of 1,371.50 $\pm$ 141.73) but not RRV-infected PBS-treated mice (mean count of 2,241.75 $\pm$ 476.27) (Fig. 8Bi and ii). Curiously, this reduction in immunocytes was in direct correlation ($P$ value of $<0.05$) to the reduced viral load observed in the muscles of RRV-infected PG545-treated mice (Fig. 8C). Although joints did not show a significant reduction in viral load between the infected PG545-treated and infected PBS-treated groups, a smaller downward trend was noted in the joints of RRV-infected PG545-treated mice.

**Therapeutic PG545 regimen exerts a modest anti-inflammatory effect by reducing the upregulation of MCP-1 and IL-6 in the muscles and HPSE in the joints of RRVD mice.** Following the musculoprotection seen in Fig. 8B and C, a further downregulation was noted in MCP-1 ($P$ value of $<0.01$) and IL-6 ($P$ value of $<0.05$) in the muscles of RRV-infected PG545-treated mice compared to those in the muscles of

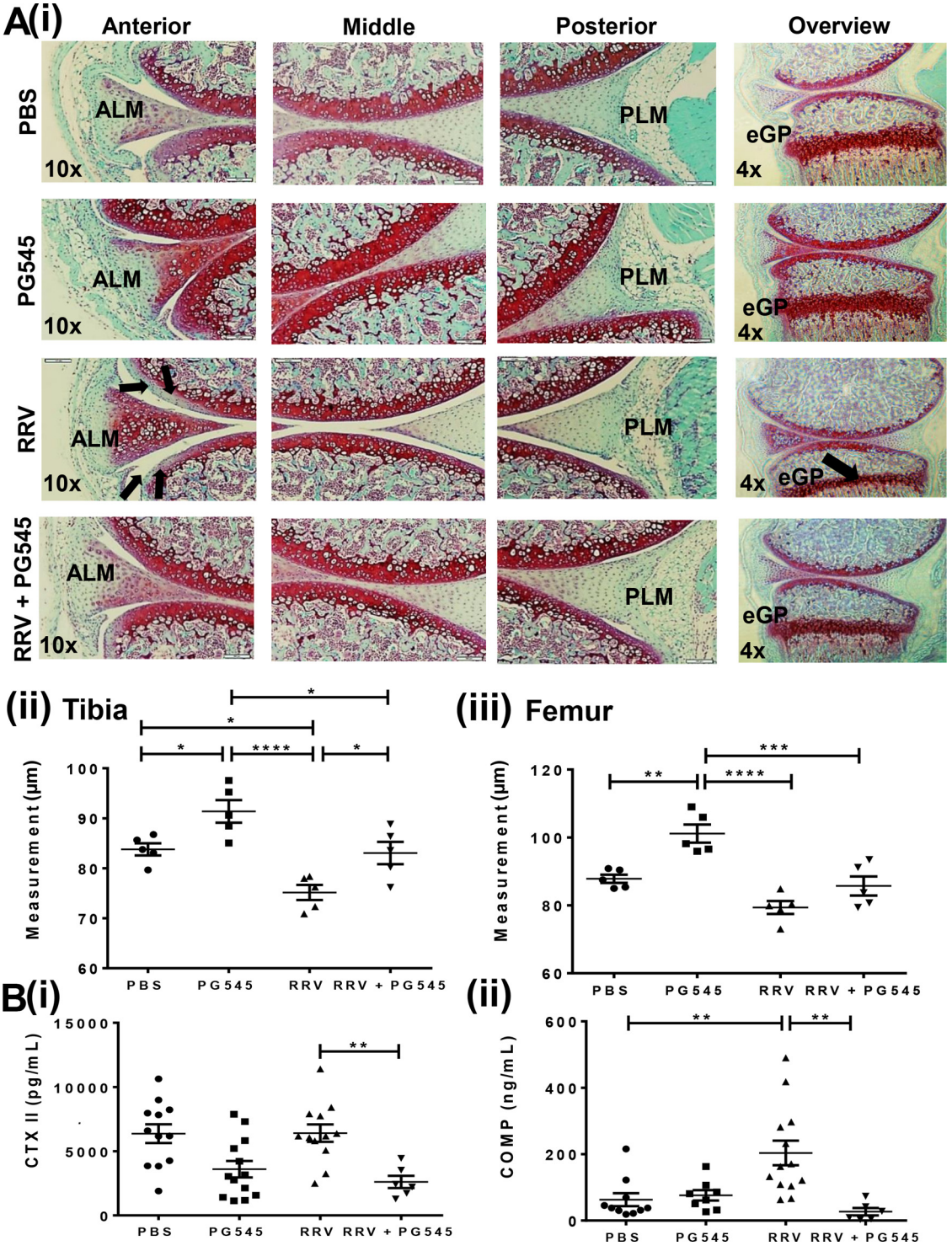


**FIG 6** Prophylactic PG545 treatment protects chondrocytes from RRV-induced cartilage damage and breakdown. (A) Knee joints were fixed in 4% PFA and then decalcified in 14% EDTA and stained with Safranin O/fast green. (Ai to iii) The width of the articular cartilage was enumerated from 6 distinct regions of the tibiofemoral cartilage interphase. (Bi and ii) Serum was used to quantify cartilage breakdown proteins. COMP and CTX-II were used in commercial sandwich ELISA kits. PBS, mock-infected PBS control; PG545, mock infected and PG545 treated; RRV, RRV infected and PBS treated; RRV + PG545, RRV infected and PG545 treated. Values are expressed as mean width ($\mu$m) or mean protein concentration (ng or pg/ml) ± SEM for 4 to 16 mice per group. SB, subchondral bone; eGP, epiphyseal growth plate; ALM, anterior lateral meniscus; PLM, posterior lateral meniscus.

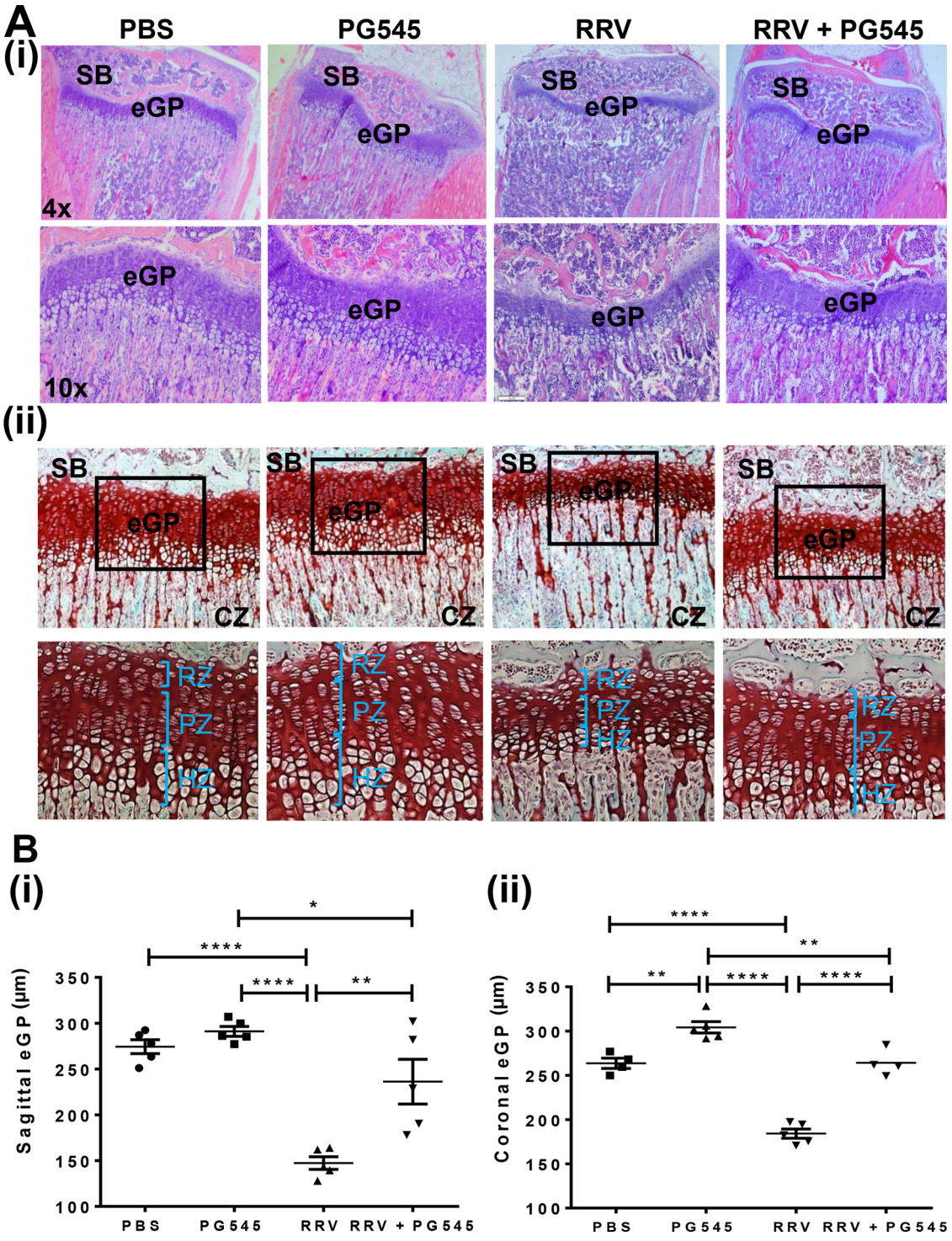


**FIG 7** Prophylactic PG545 treatment protects against RRV-induced growth plate thinning. (Ai and ii) Knee joints were fixed with 4% PFA, decalcified in 14% EDTA, and stained with either Safranin O/fast green or H&E. (Bi and ii) The width of the growth plate cartilage was enumerated at 5 distinct points to evaluate overall growth plate thickness. PBS, mock-infected PBS control; PG545, mock infected and PG545 treated; RRV, RRV infected and PBS treated; RRV + PG545, RRV infected and PG545 treated. Values are expressed as mean width ($\mu$m) $\pm$ SEM for 4 to 16 mice per group. SB, subchondral bone; eGP, epiphyseal growth plate; RZ, resting zone; PZ, proliferation zone; HZ, hypertrophic zone; CZ, calcified zone.

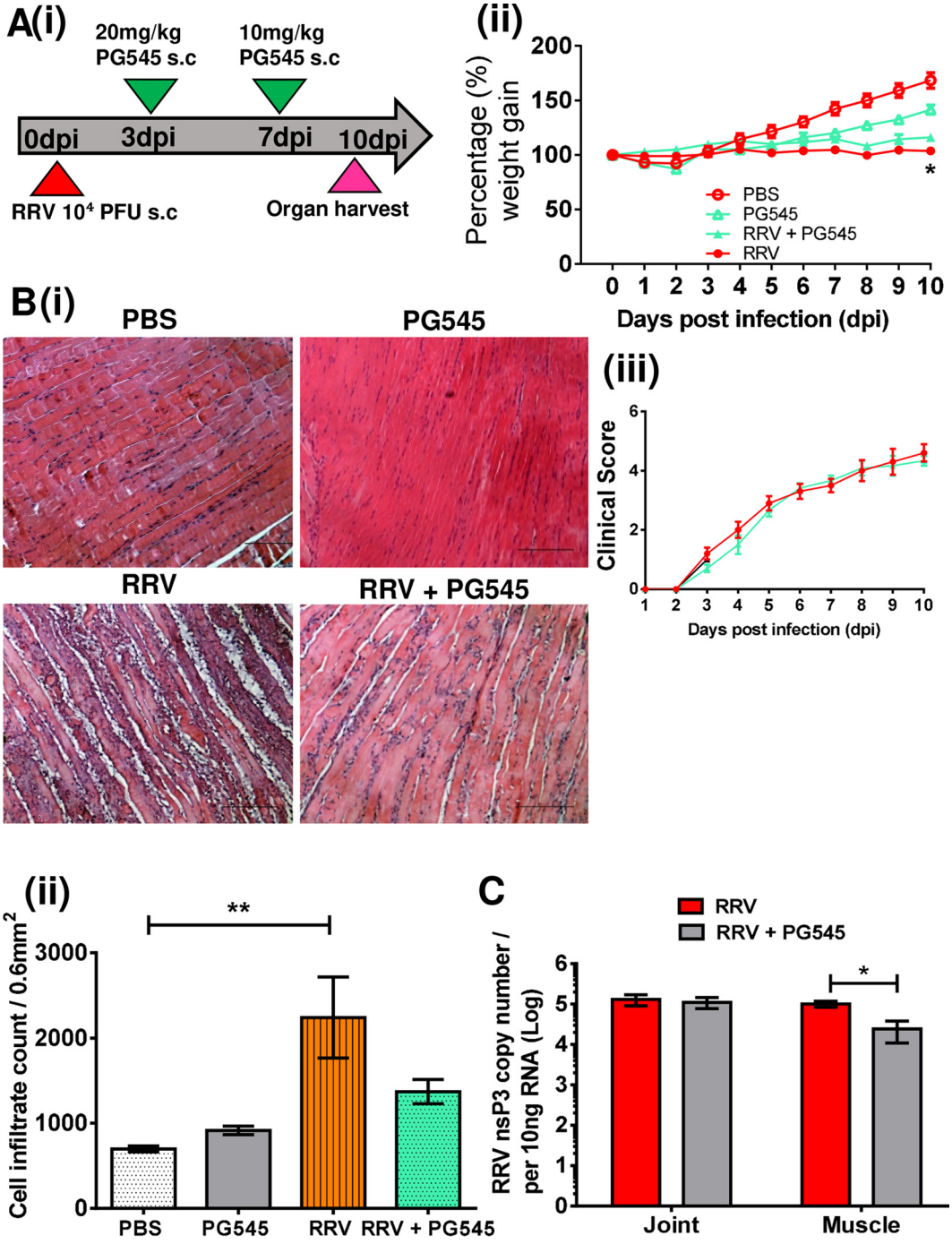


**FIG 8** Therapeutic PG545 treatment does not have any clinical outcome in mice with RRVD at peak disease but maintains an antiviral effect on tissue-bound virus. (A) In the therapeutic treatment model, 3-week-old C57BL/6 mice were infected s.c. with $10^4$ PFU/50 $\mu$l PBS or PBS alone on day 0 in the right thorax and also received s.c. injections of PG545 or mock-infected PBS 3 and 7 dpi in the right thorax. Mice were weighed and scored for disease progression as described in Materials and Methods. (B) Muscles were fixed in 4% PFA and H&E stained, and total cell infiltrate counts per section were enumerated. (C) Muscle and joints were homogenized and RNA was extracted for downstream viral genomic material analysis using nsP3 region-specific primers. For data analysis, plasmid copy numbers were extrapolated from RRV T48 standards ($n = 7$). Values are expressed as means $\pm$ SEM from 4 to 10 mice per group.

RRV-infected PBS-treated mice (Fig. 9). While there was no significant difference between all other soluble host factors across joints and muscles in both RRV-infected PG545-treated and RRV-infected PBS-treated groups, it is noteworthy that HPSE was still downregulated ($P$ value of $<0.05$) in the joints of RRV-infected PG545-treated mice

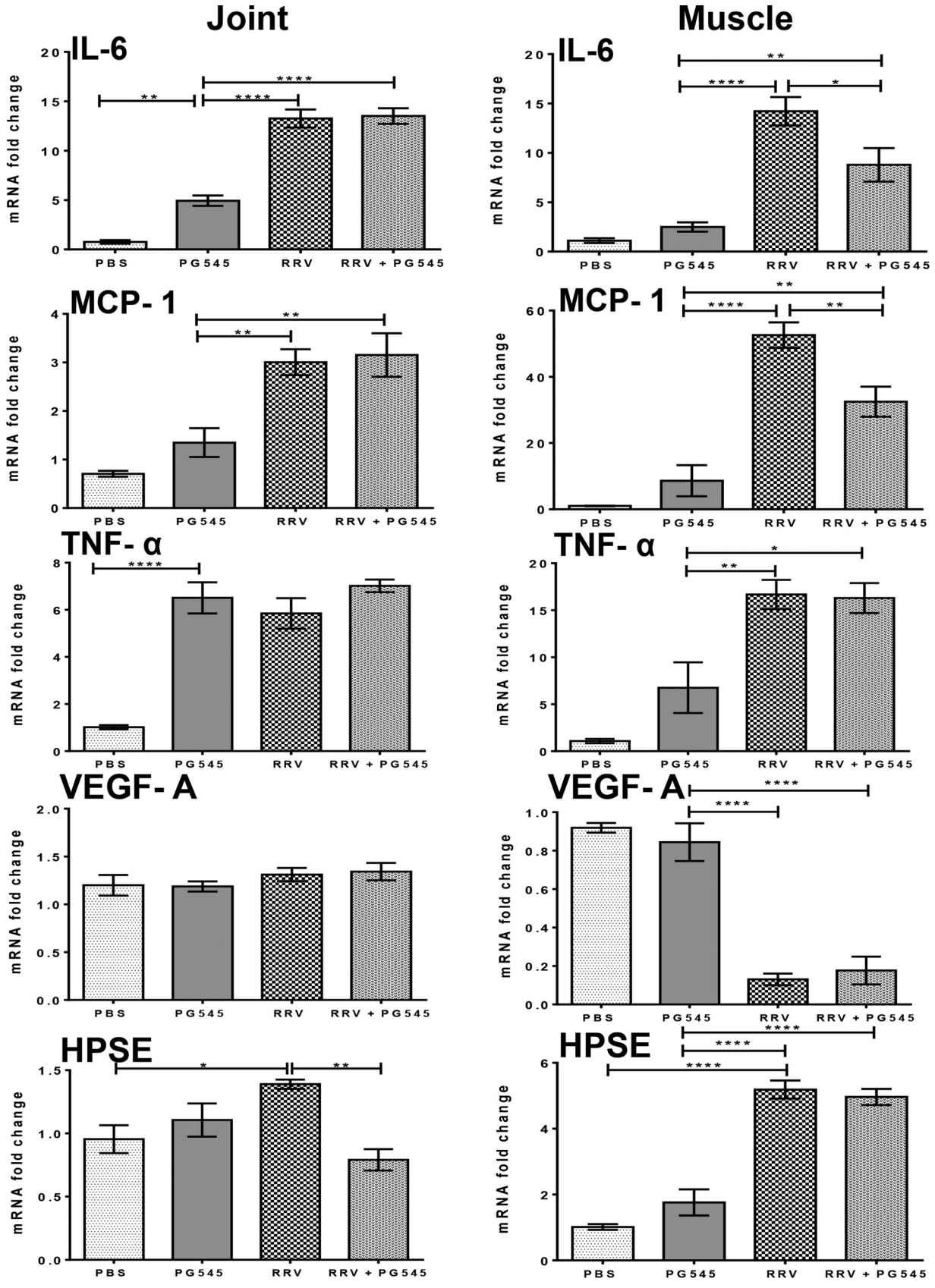


**FIG 9** Therapeutic PG545 treatment reduces upregulation of MCP-1 and IL-6 in muscles and HPSE in joints of RRVD mice. Muscles and joints were homogenized and RNA extracted to analyze soluble host factor expression via qPCR. The *y* axis is the final calibrated transcript expression,

(Continued on next page)

compared with RRV-infected PBS-treated mice. A small downward trend of HPSE was also observed in muscles of RRV-infected PG545-treated mice (Fig. 9). Overall, these postexposure findings suggest only partial anti-inflammatory and anti-HPSE effects by PG545 when administered after peak viremia.

## DISCUSSION

Certain viruses, including herpes simplex virus (HSV), dengue virus (DENV), respiratory syncytial virus (RSV), and alphaviruses such as SINV, utilize cell surface heparan sulfate proteoglycans (HSPGs) as coreceptors to anchor their viral proteins and subsequently infect healthy host cells (21, 26, 31, 32). The precise mode of entry of HS binding viruses enables HS mimetics to display a favorable antiviral or virucidal activity. As alternate virus binding HS ligands, HS mimetics can antagonize the viral attachment proteins' affinity to HSPG on the cell membrane (21). Recently, the HS mimetics suramin and PPS have demonstrated favorable disease outcomes when used to treat RRVD and/or CHIKVD in mice (16, 17). Further, PG545 has also shown high potency as a virucidal agent against both RSV and HSV-2 particles despite its initial discovery as an anticancer drug (21, 22, 33). The present study examined if a similar mode of viral inhibition could be demonstrated for PG545 with RRV, CHIKV, and BFV. Dose-dependent $IC_{50}$s were assessed on strains of RRV, CHIKV, and BFV, with PG545 showing efficacious viral inhibition on all strains tested. Previous viral studies on PG545 reported that the virucidal activity of PG545 contributes to inhibition of viral attachment to target cells and neutralization of virus, rendering the virus noninfective (21, 22). Therefore, binding interactions were assessed by evaluating the affinity and stoichiometry of PG545 binding to whole viral proteins. Results indicated efficient binding affinity between PG545 and viral protein, as demonstrated by $K_D$ values that mostly ranged from 4 ($\pm$0.42) $\mu$M to 0.25 ($\pm$0.12) $\mu$M.

We recently reported that HPSE, an endoglycosidase implicated in the pathogenic remodeling of HS proteoglycans, is upregulated in RRV-infected primary human chondrocytes and RRV-infected primary skeletal muscle cells (11). *In vivo*, we report a similar elevation of HPSE expression in both joints and muscles of RRV-infected mice. Additionally, RRV-infected PG545-treated mice also conferred a reduction in HPSE protein levels in muscles. Some studies report that HPSE remodeling of the ECM can also negatively affect immunocyte recruitment, activation, and extravasation and migration to inflamed or injured sites (34). Studies show that HPSE has a role in modulating neutrophils, macrophages, and dendritic cells in an acute inflammatory event (35). This could be due largely to its ability to cleave HS chains, releasing matrix-anchored cytokines and chemokines, thereby exacerbating the inflammatory response. Our results show that in addition to the reduction in HSPE expression, the presence of inflammatory monocytes and neutrophils (Fig. 2Ci and ii) were also remarkably reduced in the muscles of the RRV-infected PG545-treated groups. Pronounced immune infiltrate proliferation and adverse changes to the striated muscle fibers with localized necrosis to fibers (based on hematoxylin and eosin [H&E]- and phosphotungstic acid hematoxylin [PTAH]-stained tissue sections) were also observed (Fig. 2Bi and ii), while the prophylactic administration of PG545 to infected mice substantially restricted prominent leukocyte recruitment and preserved tissue morphology. A recent study reported that the upregulation of HPSE in hepatocellular carcinoma causes both tissue damage and breakdown with fibrosis, similar to the damage often observed in RRVD musculature at peak disease. The study further reports that inhibiting HPSE with suramin restored liver integrity (36). This observation suggests that the ability of PG545 to impede HPSE expression allows the maintenance of ECM and thus deters the extravasation of inflammatory cells to potentiate tissue damage. However, whether the

**FIG 9** Legend (Continued)
graphed as fold shift, and the *x* axis designates the treatment groups. PBS, mock-infected PBS control; PG545, mock infected and PG545 treated; RRV + PBS, RRV infected and PBS treated; RRV + PG545, RRV infected and PG545 treated. Values are expressed as mean mRNA fold change in expression ± SEM for 4 or 5 mice in each group.

prolific production of HPSE is a host defense reaction to the dysregulation in tissue homeostasis or a pathogenic action in tandem with proinflammatory mediators exacerbating disease states remains to be elucidated.

It was found that the expression of soluble host factors IL-6, MCP-1, IFN-$\gamma$, and TNF-$\alpha$ were either significantly reduced or followed a downward trend with the RRV-infected PG545-treated mice, while the extensively reported gene upregulation was observed in RRV-infected PBS-treated mice. Interestingly, VEGF-A upregulation was also noted in prophylactic RRV-infected PG545-treated mice, where VEGF-A has been shown to be a biomarker of PG545 response (33).

Recently it was found that RRVD joint pathology was an element contributing to viral inflammatory arthritis/disease. Studies on arthritis report that HS proteoglycan-containing collagen damage often occurs within articulating joints during diseased states (37, 38). Thus, loss of proteoglycans is a fundamental cause of matrix vulnerability and forms the framework for cartilage erosion in OA patients (37). Consistent with this, we have previously reported and currently confirm weakened proteoglycan staining on the articular cartilage lining the joints in addition to cartilage deterioration in RRV-infected PBS-treated mice, with no visible cartilage erosion in RRV-infected PG545-treated mice. Moreover, COMP, a tissue-specific protein bound to type II collagen, and CTXII, a prognostic marker for cartilage turnover, were both found to be in lower concentrations in the RRV-infected PG545-treated group than the RRV-infected PBS-treated group (39). Both COMP and CTX-II have been reported to be byproducts of joint and/or ECM deterioration and thus can be considered markers to detect the onset of OA. During damage, COMP and/or CTX-II are initially released into the synovial fluid and then enter the systemic circulation in the serum (39). Interestingly, mock-infected PBS-treated mice had an elevation of CTX-II comparable to that of RRV-infected PBS-treated mice. A study on OA in rabbits reported that the initial high elevation of CTX-II protein in young rabbits at 224 $\pm$ 118 pg/ml, which was also 20-fold higher than that in adult rabbits, is a result of growth plate activity in young animals which decreases with age. The growth plate remains active in rabbits until 12 weeks (40). Similarly, the RRV disease model consists of young mice from 3 weeks of age, which may pose a challenge to accurately distinguish cartilage or ECM breakdown using CTX-II as a marker. However, it can still be noted that the PG545 treatment has significant influence over cartilage and ECM turnover (Fig. 6 and 7). Additionally, chondroprotection and well-preserved proteoglycan staining of the hyaline structures of the lateral tibiofemoral interface, as well as the epiphyseal growth plate in RRV-infected PG545-treated mice, was noted, unlike the case for the RRV-infected PBS-treated mice. While a reduction in disease progression and hind limb dysfunction in prophylactic PG545-treated RRV-infected mice was observed, insufficient clinical benefit of PG545 treatment was noted when administered therapeutically at 3 dpi after the onset of peak viremia at 2 dpi. There were no differences in disease progression between the RRV-infected PG545-treated group and the RRV-infected mock-treated group in the therapeutic treatment regimen.

Interestingly, the regulation of VEGF-A remained only moderately elevated between the RRV-infected PG545-treated and RRV-infected PBS-treated groups. VEGF-A is an established biomarker of PG545 response. Thus, this observation led to the conclusion that the anti-heparanase and/or antiviral activity of PG545 only has partial therapeutic effects on muscles and had no effect once virus had reached peak viremia. This suggests that the compound can only act efficaciously on RRV at an entry stage, not once it has undergone several rounds of replication and amplification. The effect of this replication and any subsequent mutations/modifications to virus may contribute to this observation and require further studies. Moreover, PG545 was recently reported to be a potent prophylactic antiviral agent to HSV in animal models, demonstrating effective virucidal activity by disrupting the envelope proteins of HSV-2 (21). Although the therapeutic benefit of PG545 remains weak, it should be noted that when treated prior to viral adsorption *in vitro* and prophylactically prior to virus inoculation *in vivo*, PG545 has high antiviral potency against RRV, BFV, and CHIKV infection.

These results show a potential role of PG545 as an immune-modulating agent with antiviral and anti-inflammatory properties in a time-dependent manner. This study also provides evidence to support further studies regarding the feasibility of using PG545 prophylaxis to treat arthritogenic alphaviral disease. As PG545 is already in clinical trials, there is the potential to develop it as a prophylactic agent that could be taken prior to travel to areas where arthritogenic alphaviruses are endemic. Additionally, it could also serve as an agent that could be administered to a vulnerable population to curtail outbreaks. In conclusion, our findings demonstrate that while prophylactic PG545 treatment only mitigates acute disease, it remains antiviral in both prophylactic and therapeutic applications in mice with RRVD.

## MATERIALS AND METHODS

**Viruses and cells.** Stocks of the laboratory strain RRV T48 were generated from the full-length T48 cDNA clone (kindly provided by Richard Kuhn, Purdue University). The Asian CHIKV isolate was isolated in the early 1960s (GenBank accession number FJ457921) (30). The ECSA strain was Reunion Island isolate LR2006-OPY1 from the outbreak in Reunion Island in 2005 and was generated from an infectious clone of the primary isolate kindly provided by Andres Merits, University of Tartu, Tartu, Estonia (GenBank accession number DQ443544.2) (41). Details of BFV 2193 can be found in reference 42. All further titrations and $IC_{50}$ values were evaluated by plaque assays of Vero cells. Vero cells were grown in 3% fetal calf serum (FCS) in Opti-MEM and maintained in 1% FCS in Opti-MEM.

**$IC_{50}$ assay.** Plaque assays for $IC_{50}$ determination were performed as described previously, with some modifications (16, 21). Briefly, for $IC_{50}$ determination of previral adsorption PG545 treatment, serially diluted virus was incubated with various concentrations of PG545 (42.3 $\mu$M [100 $\mu$g/ml], 8.46 $\mu$M [20 $\mu$g/ml], 1.69 $\mu$M [4 $\mu$g/ml], 0.34 $\mu$M [0.8 $\mu$g/ml], and 0.068 $\mu$M [0.16 $\mu$g/ml]) for 20 min at room temperature. Vero cells then were adsorbed with the serially diluted virus samples alone or with virus and PG545 mixture for 1 h, after which cells were washed and 1% agar overlay was added. For $IC_{50}$ determination of PG545 treatment response to postviral adsorption, 100 $\mu$l of various compound concentrations (as described above) was added prior to wash and 1% agar overlay. Plaque assays were incubated for 2 days at 37°C and then formaldehyde fixed and stained for 30 min with 1% crystal violet to visualize plaques.

To extrapolate the $IC_{50}$s of compounds to the different field isolates, a dose-response (semilogarithmic) graph was charted. Percentage inhibition was calculated by the formula [1 − (number of plaques test compound/number of plaques control)] × 100. Percent inhibition was plotted against the various PG545 concentrations (in micromolars and micrograms per milliliter) to estimate the $IC_{50}$s. For plaque assays, virus titers were denoted as PFU/milligram of tissue or PFU/milliliter for supernatants, where PFU is characterized as a unit of infectiousness of the virus.

**Isothermal calorimetry analysis of alphavirus-PG545 interaction.** Isothermal titration calorimetry experiments were carried out with the nano-ITC low-volume calorimeter (TA Instruments). Both virus and ligand (PG545) solutions were prepared in PBS. The calorimeter was electrically calibrated according to the manufacturer's instructions. Ten million PFU of ECSA CHIKV strain, Asian CHIKV strain, BFV2193, or RRV T48 was loaded into the calorimeter cell, while the titration syringe was loaded with 8.46 to 15 $\mu$M PG545. Titrations were carried out using 20 injections of 2.5 $\mu$l each, injected at 3- to 4-min intervals at a constant temperature of 25°C. As a control experiment, PG545 was titrated into the cell with only PBS buffer. The temperatures of control blanks of PG545 in PBS alone were subtracted from those of the virus-PG545 interactions, measuring the changes in temperature caused by an injection of PG545 in diluent (PBS) alone (compound effects) and providing a single value for subtraction. Stirring was maintained at 150 rpm as suggested by the manufacturer. Analysis was performed using the NanoAnalyze program (TA Instruments). $K_D$ values were enumerated from two independent experiments and defined with standard errors of the means (SEM). Calorimetric data were plotted and fitted using the independent site binding mode.

**Compound treatment.** PG545 was prepared according to the literature (19). Treatment with PG545 or vehicle alone was given s.c. at 20 mg/kg of body weight in 100 $\mu$l PBS (vehicle) for the initial preload, while 10 mg/kg in 50 $\mu$l PBS was given as the second dose. The dosing schedule and regimen for the PG545 treatment was determined in accordance with the pharmacokinetic (PK) properties from the numerous mouse tumor models published (20, 43). Drug delivery design consisted of both prophylactic and therapeutic intervention, where prophylactic treatment was initiated 1 day prior to the virus infection and thereafter dosed at 4 dpi, while treatment was initiated after peak viremia in mice at 3 dpi in therapeutic investigations. The *in vitro* cellular cytotoxicity of PG545 was evaluated by previous studies to be from 230 $\mu$g/ml in HEp-2 cells (22) to 200 $\mu$g/ml in African green monkey kidney (GMK AH1) epithelial cells (21); therefore, we set the upper limit of our compound concentration at 100 $\mu$g/ml.

**Animal model.** C57BL/6 wild-type mice were purchased from the Animal Resources Centre (Perth, Australia) and kept in-house until the termination of experiments. All animal experiments were conducted in strict accordance with the Griffith University Animal Ethics guidelines defined by the Animal Ethics Committee. Twenty-one-day-old C57BL/6 mice were inoculated s.c. with $10^4$ PFU RRV in 50 $\mu$l of PBS in the right thorax to initiate RRVD as described previously (16). Mock-infected mice were inoculated with PBS alone. Mice were weighed and checked daily for disease signs. Early in infection, mice display mild signs of disease, such as ruffled fur with an increase in lethargy and diminished gripping ability, which progresses to a thorough loss of hind limb activity at peak disease on day 10. As outlined in

previous studies, the disease in RRV-infected mice encompasses 4 main phases, where 2 dpi is the peak viremic phase, 5 to 7 dpi the onset of disease phase, 10 dpi the peak disease phase, and 15 dpi the clinical disease recovery phase (44). Mice were euthanized via $CO_2$ asphyxiation on days 1, 3, 5, 7, and 10 postinfection for all sample analyses.

**Histology.** At sacrifice, intact mouse knee joints were harvested by resection of femur (1 cm above the patella) and tibia (0.5 cm above the ankle joint), in addition to quadriceps (muscle attached to the femur), and fixed in 4% paraformaldehyde (PFA) for 1 to 3 days for histological evaluation of overall tissue alterations, such as tissue and cellular morphologies or cellularity. Bone structures such as the knee joints were further decalcified in 14% EDTA prior to embedding in paraffin blocks. Fixed paraffin tissue blocks were sectioned either in longitudinal (quadriceps), sagittal (knee), or coronal (knee) orientation to 5-$\mu$m thickness and stained with hematoxylin and eosin (H&E), phosphotungstic acid hematoxylin (PTAH), or SAFO/fast green stain. Fast green only stains the surface layer of the articular cartilage and was used to evaluate cartilage erosion at the articulating surfaces. PTAH was used to confirm muscle necrosis and collagen breakdown. Stained slides were mounted with DPX coverslips and imaged at $\times$4, $\times$10, or $\times$20 magnifications under an Olympus BX60 microscope. The lateral femoral condyle or lateral tibial plateau cartilage thickness was measured (at $\times$100 magnification) at 6 specified points across the anterior-to-posterior regions of the cartilage. Further cartilage width was defined as the region of uncalcified cartilage and calcified cartilage regions; the areas below the tidemark were not included in the measurement. Epiphyseal widths were quantified only using the growth plates within the lateral tibia by an average of 5 different points throughout the axis of the growth plate. Each point of the width considered the regions from resting chondrocytes to the hypertrophic chondrocytes. All quantitative measurements were obtained using Cell Sens digital software and are represented as $\pm$SEM from 4 to 5 mice per group.

**Real-time PCR.** Tissues were lysed using TissueLyser II (Qiagen) prior to RNA extraction from tissue homogenates using TRIzol (Life Technologies, Melbourne, Australia) per the manufacturer's instructions. Purity and concentration of total RNA was measured using a NanoDrop 1000 spectrophotometer (Thermo Scientific, Victoria, Australia). Total RNA (20 ng/$\mu$l) was reverse transcribed to cDNA using 1 $\mu$g RNA template per sample using random nanomers and reverse transcriptase (Sigma-Aldrich, Sydney, Australia) according to the manufacturer's instructions. Converted cDNA was diluted to 10 ng/$\mu$l and stored at $-$20°C until further qPCR assay. The qPCRs were performed with a final volume of 12.5 $\mu$l for every reaction mixture using SsoAdvanced SYBR green supermix. Plates were run using a typical three-stage melt program conditioned at an initial activation step of 15 min at 95°C, followed by 40 cycles of 15 s at 95°C and 30 s at 55°C, and then a dissociation stage for 30 s at 72°C to ensure the presence of a single amplification peak. qPCR assays were performed on a CFX96 Touch real-time PCR detection system using either QuantiTect primer assay kits (Qiagen, Hilden, Germany) or primers purchased from Sigma-Aldrich to detect gene transcripts. Dissociation curves and threshold cycle ($C_T$) values were acquired using CFX Manager software to verify amplified amplicons. Relative expression of the genes of interest was quantitated using the comparative $C_T$ method, calculating differences in gene expression as a relative fold distinction between treatment groups and PBS (mock)-treated calibrator groups. The $C_T$ ratios were normalized to the $C_T$ value of the housekeeping gene (HPRT1) to give $\Delta C_T$. Briefly, $\Delta\Delta C_T = \Delta C_T$ (RRV infected) $- \Delta C_T$ (mock PBS infected), where $\Delta C_T = C_T$ (gene of interest) $- C_T$ (HPRT1). The final fold change for each gene was calculated as $2^{-\Delta\Delta CT}$.

**Viral load quantification.** A standard curve was generated using 7 serially diluted standards of RRV T48 infectious plasmid DNA. Quantification of viral loads was performed using SsoAdvanced universal probes supermix in half-volume reaction mixtures (12.5 $\mu$l) to detect nsP3 regions of the viral genomic material. Reactions were performed using a Bio-Rad CFX96 Touch real-time PCR detection system on 96-well plates as described previously. Cycler conditions were set in 2 parts, an initial PCR activation step at 95°C for 3 min for 1 cycle and a second step with a cycling protocol of 95°C for 15 s and then 60°C for 45 s for 45 cycles. A standard curve was derived from the extrapolation of viral copy numbers of amplified products from the 7 standards with known plasmid copy numbers.

**Sandwich ELISA.** The serum COMP (MBS451829; 1:5 dilution; MyBioSource) and CTX-II (MBS760453; 1:10 dilution; MyBioSource) concentrations and the muscle HPSE (MBS453434; 1:100 dilution; MyBioSource) level of each group were measured using commercial sandwich ELISA. Briefly, 100 $\mu$l standard or sample was added to each well, and the plate was taped and incubated for 120 min or 90 min at 37°C. The liquid in each well then was decanted, and 100 $\mu$l of biotinylated detection antibody working solution was added to each well. The plate was covered and incubated for 1 h at 37°C. Each well then was washed with wash buffer three times, 100 $\mu$l of horseradish peroxidase (HRP)-conjugated working solution was added to each well, and the plate was covered and incubated for 30 min at 37°C. Each well was washed with wash buffer five times, 90 $\mu$l of substrate was added to each well, and the plate was covered and incubated for 15 to 25 min at 37°C. Fifty microliters of stop solution was added to each well to stop the reaction when the wells turned a medium shade of blue. The optical density (OD) value of each well was determined immediately using a microplate reader at a wavelength of 450 nm. The COMP, CTX-II, and HPSE concentrations were calculated using the standard curve.

**Flow cytometry.** For flow cytometry, muscles were removed and processed as single-cell suspensions as described elsewhere (16). Briefly, quadriceps were enzymatically digested with 3 mg/ml collagenase IV and 1 mg/ml DNase I in 100 $\mu$l RPMI 1640 at 37°C for 1.5 h, resuspended in 3 ml RPMI, and filtered through 70- and 40-$\mu$m cell strainers prior to antibody panel staining. Cells were washed, pelleted, and counted. To determine percentages of specific leukocyte populations, cells were treated with Fc block (2.4G2; BD) for 5 min at 4°C and/or labeled with a panel of fluorochrome-conjugated anti-mouse antibodies, including anti-CD45 antibody (30-F11; eBioscience), anti-CD3-fluorescein

isothiocyanate (145-2C11; BD), anti-CD19-allophycocyanin (APC) (MB19-1; eBioscience), anti-CD11b-phycoerythrin (M1/70; BD), and anti-Gr1-APC (RB6-8C5; eBioscience) in various combinations at 4°C for 40 min in the dark. Cells were resuspended in 1,000 $\mu$l chilled fluorescence-activated cell sorting buffer (PBS plus 2% fetal calf serum) and were stained with propidium iodide dye (1 $\mu$g/ml; Sigma-Aldrich). Cells were counted on a CyAn ADP flow cytometer (Beckman Coulter). Single stained tubes were used as important control tubes for compensation of spectral overlaps. To ensure analysis was performed on viable cells only, PI-positive cells were excluded from analysis (Kaluza; Beckman Coulter). All postanalysis was performed using Kaluza software (Beckman Coulter).

**Statistical analysis.** One-way analysis of variance (ANOVA) with Tukey's or Dunnett's posttest was used for determining the differences in gene transcription fold change, tibial growth plate width, femoral condyle and tibial plateau thickness, H&E cell infiltrate count, and protein concentrations between groups. The percent weight gain and viral kinetics in target organs and viremia were assessed using two-way ANOVA with Bonferroni's posttest. Mann-Whitney U test was used to evaluate statistical significance for flow cytometry analyses, viral loads, and disease scores. All statistics were performed with GraphPad Prism 6.0, and $P$ values of $<0.05$ (*), $<0.01$ (**), $<0.001$ (***), and $<0.0001$ (****) were considered statistically significant.

## SUPPLEMENTAL MATERIAL

Supplemental material for this article may be found at https://doi.org/10.1128/AAC.01959-17.

**SUPPLEMENTAL FILE 1,** PDF file, 0.4 MB.

## ACKNOWLEDGMENTS

We thank Wendy Kelly and Helen Irving-Rodgers of the G12 Facility (QLD, Australia) for their histological expertise. We further thank Bernadette Bellette for her critical review of the manuscript.

L.J.H. is the recipient of an Australian National Health and Medical Council (NHMRC) Career Development Award (1105760). This study was supported by an NHMRC project grant awarded to L.J.H. (1081954). V.F. acknowledges support from the University of Queensland and the Australian Research Council (DP170104431).

## REFERENCES

1. Suhrbier A, La Linn M. 2004. Clinical and pathologic aspects of arthritis due to Ross River virus and other alphaviruses. Curr Opin Rheumatol 16:374–379. https://doi.org/10.1097/01.bor.0000130537.76808.26.
2. Harley D, Sleigh A, Ritchie S. 2001. Ross River virus transmission, infection, and disease: a cross-disciplinary review. Clin Microbiol Rev 14:909–932. https://doi.org/10.1128/CMR.14.4.909-932.2001.
3. Claflin SB, Webb CE. 2015. Ross River virus: many vectors and unusual hosts make for an unpredictable pathogen. PLoS Pathog 11:e1005070. https://doi.org/10.1371/journal.ppat.1005070.
4. Russell RC. 2002. Ross River virus: ecology and distribution. Annu Rev Entomol 47:1–31. https://doi.org/10.1146/annurev.ento.47.091201.145100.
5. Russell RC, Kay BH. 2004. Medical entomology: changes in the spectrum of mosquito-borne disease in Australia and other vector threats and risks, 1972-2004. Aust J Entomol 43:271–282. https://doi.org/10.1111/j.1326-6756.2004.00436.x.
6. Rezza G. 2014. Dengue and chikungunya: long-distance spread and outbreaks in naïve areas. Pathog Global Health 108:349–355. https://doi.org/10.1179/2047773214Y.0000000163.
7. Fraser J, Cunningham A, Clarris B, Aaskov J, Leach R. 1981. Cytology of synovial effusions in epidemic polyarthritis. Intern Med J 11:168–173.
8. Chen W, Foo S-S, Taylor A, Lulla A, Merits A, Hueston L, Forwood MR, Walsh NC, Sims NA, Herrero LJ. 2015. Bindarit, an inhibitor of monocyte chemotactic protein synthesis, protects against bone loss induced by chikungunya virus infection. J Virol 89:581–593. https://doi.org/10.1128/JVI.02034-14.
9. Rulli NE, Rolph MS, Srikiatkhachorn A, Anantapreecha S, Guglielmotti A, Mahalingam S. 2011. Protection from arthritis and myositis in a mouse model of acute chikungunya virus disease by bindarit, an inhibitor of monocyte chemotactic protein-1 synthesis. J Infect Dis 204:1026–1030. https://doi.org/10.1093/infdis/jir470.
10. Poo YS, Nakaya H, Gardner J, Larcher T, Schroder WA, Le TT, Major LD, Suhrbier A. 2014. CCR2 deficiency promotes exacerbated chronic erosive neutrophil-dominated chikungunya virus arthritis. J Virol 88:6862–6872. https://doi.org/10.1128/JVI.03364-13.
11. Lim E, Supramaniam A, Lui H, Coles P, Lee WS, Liu X, Rudd P, Herrero L. 2018. Chondroytes contribute to alphaviral disease pathogenesis as a source of virus replication and soluble factor production. Viruses 10:86. https://doi.org/10.3390/v10020086.
12. Ferro V. 2013. Heparan sulfate inhibitors and their therapeutic implications in inflammatory illnesses. Expert Opin Ther Targets 17:965–975. https://doi.org/10.1517/14728222.2013.811491.
13. Quiros RM, Rao G, Plate J, Harris JE, Brunn GJ, Platt JL, Gattuso P, Prinz RA, Xu X. 2006. Elevated serum heparanase-1 levels in patients with pancreatic carcinoma are associated with poor survival. Cancer 106:532–540. https://doi.org/10.1002/cncr.21648.
14. Li RW, Freeman C, Yu D, Hindmarsh EJ, Tymms KE, Parish CR, Smith PN. 2008. Dramatic regulation of heparanase activity and angiogenesis gene expression in synovium from patients with rheumatoid arthritis. Arthritis Rheum 58:1590–1600. https://doi.org/10.1002/art.23489.
15. Waterman M, Ben-Izhak O, Eliakim R, Groisman G, Vlodavsky I, Ilan N. 2007. Heparanase upregulation by colonic epithelium in inflammatory bowel disease. Modern Pathol 20:8–14. https://doi.org/10.1038/modpathol.3800710.
16. Herrero LJ, Foo S-S, Sheng K-C, Chen W, Forwood MR, Bucala R, Mahalingam S. 2015. Pentosan polysulfate: a novel glycosaminoglycan-like molecule for effective treatment of alphavirus-induced cartilage destruction and inflammatory disease. J Virol 89:8063–8076. https://doi.org/10.1128/JVI.00224-15.
17. Kuo S-C, Wang Y-M, Ho Y-J, Chang T-Y, Lai Z-Z, Tsui P-Y, Wu T-Y, Lin C-C. 2016. Suramin treatment reduces chikungunya pathogenesis in mice. Antiviral Res 134:89–96. https://doi.org/10.1016/j.antiviral.2016.07.025.
18. Sanderson R, Beata C, Flipo R, Genevois J, Macias C, Tacke S, Vezzoni A, Innes J. 2009. Systematic review of the management of canine osteoarthritis. Vet Rec 164:418. https://doi.org/10.1136/vr.164.14.418.
19. Ferro V, Liu L, Johnstone KD, Wimmer N, Karoli T, Handley P, Rowley J, Dredge K, Li CP, Hammond E. 2012. Discovery of PG545: a highly potent and simultaneous inhibitor of angiogenesis, tumor growth, and metastasis. J Med Chem 55:3804–3813. https://doi.org/10.1021/jm201708h.
20. Dredge K, Hammond E, Handley P, Gonda T, Smith M, Vincent C, Brandt R, Ferro V, Bytheway I. 2011. PG545, a dual heparanase and angiogenesis

inhibitor, induces potent anti-tumour and anti-metastatic efficacy in preclinical models. Br J Cancer 104:635–642. https://doi.org/10.1038/bjc.2011.11.
21. Said JS, Trybala E, Görander S, Ekblad M, Liljeqvist J-Å Jennische E, Lange S, Bergström T. 2016. The cholestanol-conjugated sulfated oligosaccharide PG545 disrupts the lipid envelope of herpes simplex virus particles. Antimicrob Agents Chemother 60:1049–1057. https://doi.org/10.1128/AAC.02132-15.
22. Lundin A, Bergström T, Andrighetti-Fröhner CR, Bendrioua L, Ferro V, Trybala E. 2012. Potent anti-respiratory syncytial virus activity of a cholestanol-sulfated tetrasaccharide conjugate. Antiviral Res 93:101–109. https://doi.org/10.1016/j.antiviral.2011.11.002.
23. Said J, Trybala E, Andersson E, Johnstone K, Liu L, Wimmer N, Ferro V, Bergström T. 2010. Lipophile-conjugated sulfated oligosaccharides as novel microbicides against HIV-1. Antiviral Res 86:286–295. https://doi.org/10.1016/j.antiviral.2010.03.011.
24. Ekblad M, Adamiak B, Bergstrom T, Johnstone KD, Karoli T, Liu L, Ferro V, Trybala E. 2010. A highly lipophilic sulfated tetrasaccharide glycoside related to muparfostat (PI-88) exhibits virucidal activity against herpes simplex virus. Antiviral Res 86:196–203. https://doi.org/10.1016/j.antiviral.2010.02.318.
25. Heil ML, Albee A, Strauss JH, Kuhn RJ. 2001. An amino acid substitution in the coding region of the E2 glycoprotein adapts Ross River virus to utilize heparan sulfate as an attachment moiety. J Virol 75:6303–6309. https://doi.org/10.1128/JVI.75.14.6303-6309.2001.
26. Zhu W, Wang L, Yang Y, Jia J, Fu S, Feng Y, He Y, Li J-P, Liang G. 2010. Interaction of E2 glycoprotein with heparan sulfate is crucial for cellular infection of Sindbis virus. PLoS One 5:e9656. https://doi.org/10.1371/journal.pone.0009656.
27. Mihaila R, Nedelcu L, Fratila O, Rezi EC, Domnariu C, Ciuca R, Zaharie AV, Olteanu A, Bera L, Deac M, Mihaila R. 2009. Lovastatin and fluvastatin reduce viremia and the pro-inflammatory cytokines in the patients with chronic hepatitis C. Hepatogastroenterology 56:1704–1709.
28. Schul W, Liu W, Xu HY, Flamand M, Vasudevan SG. 2007. A dengue fever viremia model in mice shows reduction in viral replication and suppression of the inflammatory response after treatment with antiviral drugs. J Infect Dis 195:665–674. https://doi.org/10.1086/511310.
29. Morrison TE, Whitmore AC, Shabman RS, Lidbury BA, Mahalingam S, Heise MT. 2006. Characterization of Ross River virus tropism and virus-induced inflammation in a mouse model of viral arthritis and myositis. J Virol 80:737–749. https://doi.org/10.1128/JVI.80.2.737-749.2006.
30. Gardner J, Anraku I, Le TT, Larcher T, Major L, Roques P, Schroder WA, Higgs S, Suhrbier A. 2010. Chikungunya virus arthritis in adult wild-type mice. J Virol 84:8021–8032. https://doi.org/10.1128/JVI.02603-09.
31. Chen Y, Maguire T, Hileman RE, Fromm JR, Esko JD, Linhardt RJ, Marks RM. 1997. Dengue virus infectivity depends on envelope protein binding to target cell heparan sulfate. Nat Med 3:866–871. https://doi.org/10.1038/nm0897-866.
32. Feldman SA, Audet S, Beeler JA. 2000. The fusion glycoprotein of human respiratory syncytial virus facilitates virus attachment and infectivity via an interaction with cellular heparan sulfate. J Virol 74:6442–6447. https://doi.org/10.1128/JVI.74.14.6442-6447.2000.
33. Winterhoff B, Freyer L, Hammond E, Giri S, Mondal S, Roy D, Teoman A, Mullany SA, Hoffmann R, von Bismarck A, Chien J, Block MS, Millward M, Bampton D, Dredge K, Shridhar V. 2015. PG545 enhances anti-cancer activity of chemotherapy in ovarian models and increases surrogate biomarkers such as VEGF in preclinical and clinical plasma samples. Eur J Cancer 51:879–892. https://doi.org/10.1016/j.ejca.2015.02.007.
34. Lever R, Rose MJ, McKenzie EA, Page CP. 2014. Heparanase induces inflammatory cell recruitment in vivo by promoting adhesion to vascular endothelium. Am J Physiol Cell Physiol 306:C1184–C1190. https://doi.org/10.1152/ajpcell.00269.2013.
35. Sasaki N, Higashi N, Taka T, Nakajima M, Irimura T. 2004. Cell surface localization of heparanase on macrophages regulates degradation of extracellular matrix heparan sulfate. J Immunol 172:3830–3835. https://doi.org/10.4049/jimmunol.172.6.3830.
36. Tayel A, El Galil KHA, Ebrahim MA, Ibrahim AS, El-Gayar AM, Al-Gayyar MM. 2014. Suramin inhibits hepatic tissue damage in hepatocellular carcinoma through deactivation of heparanase enzyme. Eur J Pharmacol 728:151–160. https://doi.org/10.1016/j.ejphar.2014.02.001.
37. Rizkalla G, Reiner A, Bogoch E, Poole A. 1992. Studies of the articular cartilage proteoglycan aggrecan in health and osteoarthritis. Evidence for molecular heterogeneity and extensive molecular changes in disease. J Clin Investig 90:2268.
38. Noss EH, Brenner MB. 2008. The role and therapeutic implications of fibroblast-like synoviocytes in inflammation and cartilage erosion in rheumatoid arthritis. Immunol Rev 223:252–270. https://doi.org/10.1111/j.1600-065X.2008.00648.x.
39. Bai B, Li Y. 2016. Combined detection of serum CTX-II and COMP concentrations in osteoarthritis model rabbits: an effective technique for early diagnosis and estimation of disease severity. J Orthop Surg Res 11:149. https://doi.org/10.1186/s13018-016-0483-x.
40. Duclos M, Roualdes O, Cararo R, Rousseau J, Roger T, Hartmann D. 2010. Significance of the serum CTX-II level in an osteoarthritis animal model: a 5-month longitudinal study. Osteoarthritis Cartilage 18:1467–1476. https://doi.org/10.1016/j.joca.2010.07.007.
41. Tsetsarkin K, Higgs S, McGee CE, De Lamballerie X, Charrel RN, Vanlandingham DL. 2006. Infectious clones of Chikungunya virus (La Reunion isolate) for vector competence studies. Vector Borne Zoonotic Dis 6:325–337. https://doi.org/10.1089/vbz.2006.6.325.
42. Herrero LJ, Lidbury BA, Bettadapura J, Jian P, Herring BL, Hey-Cunningham WJ, Sheng KC, Zakhary A, Mahalingam S. 2014. Characterization of Barmah Forest virus pathogenesis in a mouse model. J Gen Virol 95:2146–2154. https://doi.org/10.1099/vir.0.064733-0.
43. Hammond E, Brandt R, Dredge K. 2012. PG545, a heparan sulfate mimetic, reduces heparanase expression in vivo, blocks spontaneous metastases and enhances overall survival in the 4T1 breast carcinoma model. PLoS One 7:e52175. https://doi.org/10.1371/journal.pone.0052175.
44. Foo SS, Chen W, Taylor A, Sheng KC, Yu X, Teng TS, Reading PC, Blanchard H, Garlanda C, Mantovani A, Ng LF, Herrero LJ, Mahalingam S. 2015. Role of pentraxin 3 in shaping arthritogenic alphaviral disease: from enhanced viral replication to immunomodulation. PLoS Pathog 11:e1004649. https://doi.org/10.1371/journal.ppat.1004649.
45. Morrison TE, Fraser RJ, Smith PN, Mahalingam S, Heise MT. 2007. Complement contributes to inflammatory tissue destruction in a mouse model of Ross River virus-induced disease. J Virol 81:5132–5143. https://doi.org/10.1128/JVI.02799-06.